Biochimica et Biophysica Acta 1817 (2012) 1213–1219

Contents lists available at SciVerse ScienceDirect

Biochimica et Biophysica Acta

journal homepage: www.elsevier.com/locate/bbabio

Temperature-dependent vibrational and conformational dynamics of photosystem II membrane fragments from spinach investigated by elastic and inelastic neutron scattering ☆

Jörg Pieper [a,*], Marcus Trapp [b,c,1], Andrei Skomorokhov [d,e], Ireneusz Natkaniec [d], Judith Peters [b,c,f], Gernot Renger [g]

[a] Institute of Physics, University of Tartu, Riia 142, 51014 Tartu, Estonia
[b] Institut Laue-Langevin, P.O. Box 156, 38042 Grenoble Cedex 9, France
[c] Université Joseph Fourier Grenoble I, UFR PhITEM, 38041 Grenoble Cedex 9, France
[d] Frank Laboratory of Neutron Physics, JINR, Dubna, Russia
[e] Institute for Physics and Power Engineering, Obninsk, Russia
[f] Institut de Biologie Structurale, 38027 Grenoble Cedex 1, France
[g] Max-Volmer-Laboratories for Biophysical Chemistry, Technical University, Strasse des 17, Juni 135, 10623 Berlin, Germany

ARTICLE INFO

Article history:
Received 7 February 2012
Received in revised form 7 March 2012
Accepted 16 March 2012
Available online 23 March 2012

Keywords:
Elastic neutron scattering
Inelastic neutron scattering
Photosystem II
Protein vibration
Excitation energy transfer
Electron transfer

ABSTRACT

Vibrational and conformational protein dynamics of photosystem II (PS II) membrane fragments from spinach were investigated by elastic and inelastic incoherent neutron scattering (EINS and IINS). As to the EINS experiments, the average atomic mean square displacement values of PS II membrane fragments hydrated at a relative humidity of 57% exhibit a dynamical transition at ~230 K. In contrast, the dynamical transition was absent at a relative humidity of 44%. These findings are in agreement with previous studies which reported a "freezing" of protein mobility due to dehydration (Pieper et al. (2008) Eur. Biophys. J. 37: 657–663) and its correlation with an inhibition of electron transfer from $Q_A^{-\bullet}$ to Q_B (Kaminskaya et al. (2003) Biochemistry 42, 8119–8132). IINS spectra of a sample hydrated at a relative humidity of 57% show a distinct Boson peak at ~7.5 meV at 20 K, which shifts towards lower energy values upon temperature increase to 250 K. This unexpected effect is interpreted in terms of a "softening" of the protein matrix along with the onset of conformational protein dynamics as revealed by the EINS experiments. Information on the density of vibrational states of pigment–protein complexes is important for a realistic calculation of excitation energy transfer kinetics and spectral lineshapes and is often routinely obtained by optical line-narrowing spectroscopy at liquid helium temperature. The data presented here demonstrate that IINS is a valuable experimental tool in determining the density of vibrational states not only at cryogenic, but also at nearly physiological temperatures up to 250 K. This article is part of a Special Issue entitled: Photosynthesis Research for Sustainability: from Natural to Artificial.

1. Introduction

Functionalizing of pigments and other cofactors by suitable incorporation into protein matrices is of key relevance for the efficient exploitation of solar radiation as unique source of Gibbs free energy through the process of photosynthesis. During evolution two classes of pigment–protein complexes with distinctly different functions have been developed: i) antenna complexes and ii) reaction centers (RCs). These operational units perform the light driven processes of photosynthesis in a well controlled and highly efficient manner. The pigments of the antenna complexes (for reviews, see [1–3]) absorb light and transfer the electronic excitation energy via radiation-less excitation energy transfer (EET) to the photochemically active pigment(s) of the RCs where the transformation into electrochemical free energy takes place (for a review, see [4]). The functional competence of these operational units primarily depends on a suitable

Abbreviations: EINS, elastic incoherent neutron scattering; EISF, elastic incoherent structure factor; EET, excitation energy transfer; FLN, fluorescence line-narrowing; HB, hole burning; HWHM, half-width at half maximum; IINS, inelastic incoherent neutron scattering; LAMP, Large Array Manipulation Program; LHC II, light-harvesting complex II; MD, molecular dynamics; NHFe, non-heme iron; OEC, oxygen evolving complex; PBRC, reaction center of purple bacteria; r.h., relative humidity; PS II, photosystem II; QENS, quasielastic neutron scattering; QISF, quasielastic incoherent structure factor; RC, reaction center

☆ This article is part of a Special Issue entitled: Photosynthesis Research for Sustainability: from Natural to Artificial.

* Corresponding author. Tel.: +372 7374627.
E-mail address: jorg.pieper@ut.ee (J. Pieper).

[1] Present address: Applied Physical Chemistry, University of Heidelberg, 69120 Heidelberg, Germany and Helmholtz-Zentrum für Materialien und Energie GmbH, 14109 Berlin, Germany.

0005-2728/$ – see front matter © 2012 Elsevier B.V. All rights reserved.
doi:10.1016/j.bbabio.2012.03.020

three-dimensional static array of the cofactors, but in many cases it also requires a certain degree of internal flexibility of the protein environment provided by harmonic vibrational and localized diffusive motions between conformational substates.

As to vibrational motions, the function of antenna complexes relies on efficient and fast EET processes which are tuned via the coupling of the electronic transitions of pigments to low-frequency vibrations of the protein matrix, also referred to as electron–phonon coupling (for reviews see [3,5]). So far, electron–phonon coupling has been primarily studied by optical spectroscopy at low temperatures, i.e. spectral hole burning (HB) and fluorescence line-narrowing (FLN) (for reviews see [3,6]). HB employs quasi-monochromatic laser light to induce conformational changes in the protein environment of a chromophore at cryogenic temperature resulting in a change or "hole" in the absorption spectrum at the burn frequency. Analysis of electron–phonon coupling is mainly based on the observation of so-called phonon sideband holes beside the actual burn frequency. The electron–phonon coupling strength observed for antenna complexes is generally weak or moderate with Huang–Rhys factors S in the range of up to 1–1.5, while the one-phonon profiles are typically strongly asymmetric with peak frequencies of values of 20–30 cm^{-1} (see e.g. [3] and references therein). In practice, however, experimental techniques like HB and FLN spectra are restricted to temperatures below ~40 K [7], because they require a static (frozen) ensemble of conformational substates. As a consequence, electron phonon coupling cannot be studied at elevated (i.e. at temperatures higher than accessible by HB and FLN) or even physiological temperatures and thus requires the application of an independent experimental approach to study the vibrational density of states of photosynthetic pigment–protein complexes.

The importance of diffusive (conformational) protein dynamics for individual redox reactions in photosynthesis is illustrated by a strong dependence on temperature and hydration of these processes in photosystem II (PS II) where the essential steps of solar energy exploitation by water splitting take place [4]. While the light-induced charge separation leading to formation of the radical ion pair $P680^{+\bullet}Q_A^{\bullet}$ remains active even at very low temperatures [8], the reoxidation of $Q_A^{-\bullet}$ by Q_B is completely blocked below 200 K [9–11] and the individual redox steps of the water oxidizing complex exhibit a characteristic temperature dependence (for a compilation of data, see [12]). Furthermore, the hydration level strongly affects $Q_A^{-\bullet}$ reoxidation [13] and the redox steps of the water oxidizing complex [14]. Therefore, the unraveling of correlations between protein dynamics and function is of high relevance for a deeper understanding of these processes.

Inelastic and elastic incoherent neutron scattering (EINS and IINS) are powerful experimental tools for direct investigations of vibrational and conformational dynamics. Because of the high incoherent scattering cross section of hydrogen atoms, which are almost homogeneously distributed in biomolecules, IINS is widely used to study vibrational dynamics of proteins (for a review, see [15]). IINS spectra of proteins generally display a distinct peak centered at energy transfers of 2–7 meV representing an excess of vibrational modes compared to the Debye-like density of states (see e.g. [16,17]). The origin of this so-called "Boson peak" is not yet fully clarified, however, it is widely accepted that it is related to the disordered nature of protein systems. Furthermore, the effective density of states can be derived from IINS spectra (see e.g. [16,17]), which permits comparison to molecular dynamics (MD) simulations of internal protein motions [18]. In photosynthesis research, IINS has so far only been employed to study protein vibrations of the major light-harvesting complex of photosystem II (LHC II) [17]. The data revealed a broad and widely asymmetric Boson peak with a maximum around ~2.5 meV, which was shown to be in good agreement with the results from HB and FLN experiments [19,20]. However, in order to ensure a proper comparison between the results of the different experimental techniques, the IINS experiments have so far been limited to temperatures below ~120 K.

At higher or even physiological temperature, localized diffusive motions between conformational substates of a protein become possible (see e.g. [21]). This type of protein dynamics has been intensively studied using elastic and quasielastic neutron scattering (QENS) (see e.g. [22–24]). A number of QENS studies have revealed that proteins undergo a drastic change in their flexibility with the onset of localized diffusive protein motions on the picosecond timescale at temperatures of about 230 K in aqueous solution, which is referred to as "dynamical transition" [25]. The origin of the dynamical transition is still largely debated and possible explanations include a sudden change in effective elasticity of proteins [26], a correlation with the onset of translational motions of bound water molecules [27], a fragile-to-strong transition of the hydration water [28], instrumental resolution effects [29,30] and a glass transition in the hydration shell [31]. Similar effects have also been observed for the purple membrane of *Halobacterium salinarum* [22,32], lipid-bilayers as well as lipid–protein systems [33]. In addition, both, transition temperature and extent of the induced protein flexibility vary with external factors like hydration [32,34–36], lipid/protein ratio of the membrane [37], or solvent viscosity [38–40].

Protein dynamics in PS II membrane fragments from spinach has recently been investigated by QENS in the temperature range between 5 and 340 K [41–44]. The "dynamical transition" in PS II membrane fragments hydrated at 90% r.h. is observed at ~240 K at a time resolution of ~20 ps [41] and was shown to be strictly correlated with the temperature-dependent increase of the electron transport efficiency from $Q_A^{-\bullet}$ to Q_B [10,11]. The dynamics of PSII membrane fragments between 280 and 340 K reveals the presence of a hydration-sensitive transition in the sample between 310 and 320 K that was attributed to the detachment of the oxygen evolving complex (OEC) [44]. At room temperature, protein dynamics was shown to be suppressed below hydration values of 44% r.h. [42], which is in agreement with the blockage of $Q_A^{-\bullet}$ reoxidation by Q_B upon dehydration of PS II [13]. So far, however, a detailed investigation of the hydration-dependence of protein dynamics in PS II membrane fragments by QENS is lacking.

In the present study, we extend our IINS measurements on photosynthetic pigment–protein complexes to temperatures higher than 120 K and, especially, almost to physiologically relevant temperatures. Experiments are carried out using PS II membrane fragments, which contain both LHC II and PS II core complexes. This sample material is used for two reasons: a) availability in relatively large quantities and b) the possibility of equilibration at defined hydration levels, which permits a better comparison to EINS and IINS experiments on conformational dynamics. In the first part, we report EINS results on PS II membrane fragments hydrated at 44 and 57% r.h., respectively. These experiments permit an identification of the dynamical transition from purely harmonic to conformational protein dynamics. In the second part, results of IINS experiments are presented, which provide information on the shape of the distribution of vibrational states in PS II membrane fragments in the different temperature ranges determined in previous EINS studies. The combination of the two techniques allows correlating the temperature dependence of the Boson peak with conformational protein dynamics.

2. Materials and methods

2.1. Sample preparation

PS II membrane fragments were isolated from spinach (*Spinacea oleracea*) following the procedure described by Berthold et al. [45] with modifications according to Völker et al. [46]. All samples were washed three times in a buffer solution containing D_2O, 50 mM MES (pD 6.5), 0.4 M sucrose, 15 mM NaCl, and 10 mM $CaCl_2$. Finally, the sample material was divided into two batches of 250 mg each and equilibrated using D_2O vapors at relative humidity (r.h.) values of

44 and 57% r.h., respectively. Buffer samples were also equilibrated at 44 and 57% r.h., respectively, i.e. under identical conditions for separate measurements. The samples were contained in vacuum-tight cylindrical slab cells with a diameter of 50 mm after equilibration in order to maintain the hydration level.

2.2. EINS measurements

Elastic incoherent neutron scattering measurements were carried out on the backscattering spectrometer IN13 [47] at the Institut Laue-Langevin (ILL) in Grenoble, France. Using an incident neutron wavelength of 2.23 Å (~16 meV), the instrument provides an almost Q-independent energy resolution of 8 μeV yielding a time resolution of about 100 ps in a momentum transfer range of 0.19–4.9 $Å^{-1}$. Experiments were performed in the temperature range of 100–280 K using data acquisition times of 1–2 h at each temperature step. The sample cells were oriented at an angle of 135° relative to the incoming neutron beam. The measured data were normalized to the incoming flux, corrected for the contribution of the empty cell and normalized using the purely incoherent scattering of a vanadium sample. The data reduction was performed using the Large Array Manipulation Program (LAMP), developed at the ILL [48].

2.3. IINS measurements

Inelastic incoherent neutron scattering measurements were performed using the time-of-flight inverted geometry spectrometer NERA [49] at the IBR-2 high flux pulsed reactor at JINR Dubna, Russia. The incident neutron energies are determined by measuring the neutron time-of-flight along the IBR-2 moderator to sample distance of 109.05 m. IINS spectra are recorded simultaneously for all wavelengths/energies at scattering angles between 20° and 160°. The energy of scattered neutrons is selected by cooled beryllium filters and pyrolytic graphite neutron wavelength analyzers placed before the detectors. The elastic peak of the analyzers was fixed at a neutron wavelength of 4.2 Å corresponding to a final energy of the scattered neutrons of 4.53 meV. The measured IINS spectra are normalized to the monitor, corrected for cryostat and empty cell contribution and finally summed over all 15 recorded scattering angles. The resolution was 0.7 meV at the elastic line and about 2–3% in the energy transfer range of 5–100 meV.

Further IINS experiments at room temperature were carried out at the time-of-flight spectrometer DIN-2PI at JINR Dubna, Russia. IINS spectra were recorded as a function of momentum transfer Q using an incident neutron wavelength of ~2.63 Å (~11.85 meV) in an elastic Q-range of 0.26–4.22 $Å^{-1}$. The elastic energy resolution of $\Delta E = 0.88$ meV was determined by vanadium standard runs. The IINS data were transferred to energy scale and subsequently corrected for detector efficiency and normalized based on the elastic intensity of vanadium runs.

2.4. Theoretical background

The number of neutrons scattered into a solid angle element δΩ and an energy transfer element δω in an incoherent neutron scattering experiment is given by [50]:

$$\frac{\delta^2\sigma}{\delta\Omega\delta\omega} = N\frac{|\mathbf{k_1}|}{|\mathbf{k_0}|}\left[b_{inc}^2 S_{inc}(\mathbf{Q},\omega)\right]. \quad (1)$$

In this expression, N is the number of scatterers, while $\mathbf{k_0}$ and $\mathbf{k_1}$ are the wave vectors of the incident and scattered neutrons, respectively, b_{inc} is the incoherent scattering length, $S_{inc}(\mathbf{Q},\omega)$ is the incoherent scattering function with $\mathbf{Q}$ being the momentum transfer defined by $\mathbf{Q} = \mathbf{k_1} - \mathbf{k_0}$ and ħω reflects the energy transfer.

In a practical experiment, $S_{inc}(\mathbf{Q},\omega)$ needs to be replaced by an experimental scattering function $S_{exp}(\mathbf{Q},\omega)$ with:

$$S_{exp}(\mathbf{Q},\omega) = F_N \exp\left(-\frac{\hbar\omega}{2kT}\right) R(\mathbf{Q},\omega)\otimes S_{theo}(\mathbf{Q},\omega), \quad (2)$$

which is composed of a normalization factor F_N, the detailed balance factor $\exp\left[-\frac{\hbar\omega}{2kT}\right]$, and the convolution of an experimentally obtained resolution function $R(\mathbf{Q},\omega)$ with a theoretical model function $S_{theo}(\mathbf{Q},\omega)$ describing the dynamics of the sample system. The latter expression typically takes the form:

$$S_{theo}(\mathbf{Q},\omega) = e^{-\langle u^2\rangle Q^2}\left\{A_0(\mathbf{Q})\delta(\omega) + \sum_n A_n(\mathbf{Q})L_n(H_n,\omega) + S_{in}(\mathbf{Q},\omega)\right\}, \quad (3)$$

which consists of three major contributions: i) a δ(ω)-shaped elastic component, ii) a sum of quasielastic Lorentzian-shaped components $L_n(H_n,\omega)$ with half-width at half maximum (HWHM) H_n, and iii) an inelastic part $S_{in}(\mathbf{Q},\omega)$ describing low-frequency vibrational motions. The fractional intensities of the elastic and quasielastic contributions are denoted by the elastic and quasielastic incoherent structure factors (EISF and QISF), $A_0(Q)$ and $A_n(Q)$, respectively. The term $e^{-\langle u^2\rangle Q^2}$ is the Debye-Waller factor characterized by the "global" vibrational mean square displacement $\langle u^2\rangle$.

Instead of the phenomenological scattering function described above, the Q-dependence of the EISF $A_0(Q)$ can be fitted using special dynamical models, e.g. by the so-called double-well jump model [51]:

$$A_0(Q) = 1 - 2p_1p_2\left(1 - \frac{\sin(Qd)}{Qd}\right), \quad (4)$$

where p_1 and p_2 (with $p_1 = 1 - p_2$) are the occupation probabilities of the ground and the excited state, and d is the spatial distance between the two potential wells symbolizing a simplified description of the energy landscape of a biomolecule.

EINS experiments are typically analyzed in terms of the Gaussian approximation so that the elastic incoherent scattering function reduces to [25]:

$$S(Q,\omega = 0 \pm \Delta E) \approx I_0\, e^{-\langle u^2\rangle Q^2} \quad (5)$$

where $\langle u^2\rangle$ is the average atomic mean square displacement. Thus, the value of $\langle u^2\rangle$ at a given temperature can be obtained from the slope of a semi-logarithmic plot of the elastic intensity according to:

$$\langle u^2\rangle = -\frac{d\ln S(Q,0\pm\Delta E)}{dQ^2}. \quad (6)$$

In an IINS experiment, assuming the absence of quasielastic scattering (i.e. at temperatures below the dynamical transition of a given system), S (Q,ω) is given by [52]:

$$S(Q,\omega) = e^{-\langle u^2\rangle Q^2}\delta(\omega) + \frac{\langle u^2\rangle Q^2}{1!}S_1(\omega) + \frac{\left[\langle u^2\rangle Q^2\right]^2}{2!}S_2(\omega) + \ldots + \frac{\left[\langle u^2\rangle Q^2\right]^R}{R!}S_R(\omega) + \ldots$$

Here, the first term $\delta(\omega)$ represents the purely elastic scattering, while the $S_R(\omega)$-terms correspond to R-phonon transitions ($R = 1$,

2, …). If a one-phonon approximation is employed, which is valid for the small values of $\langle u^2 \rangle$ and Q^2 Eq. (7) reduces to [50]:

$$S(Q,\omega) = e^{-\langle u^2 \rangle Q^2} \left\{ \delta(\omega) + \langle u^2 \rangle Q^2 S_1(\omega) \right\}. \quad (8)$$

In amorphous systems like proteins and membranes, one typically observes a strongly asymmetric one-phonon profile designated as "Boson peak" (see e.g. [16,17]). In the present paper, we therefore employ one-phonon functions composed of a Gaussian shape at its low-energy wing and a more slowly tailing Lorentzian shape at its high-energy side [7].

3. Results and discussion

3.1. EINS experiments

In order to characterize localized conformational dynamics, temperature-dependent EINS experiments were carried out on PS II membrane fragment samples equilibrated at hydration levels of 44 and 57% r.h. The latter hydration values were chosen, because previous QENS experiments indicated the onset of conformational dynamics above 44% r.h. at room temperature [42], while temperature-dependent QENS experiments have only been performed for samples hydrated at 90% r.h. or dried in vacuum [41]. Thus, information on the dynamical transition for intermediate hydration levels is so far lacking.

The average atomic mean square displacements $\langle u^2 \rangle$ shown in Fig. 1 were extracted from semi-logarithmic plots of the elastic scattering intensity as a function of Q^2 according to Eq. (6) (not shown). Before determination of the $\langle u^2 \rangle$-values, the buffer data were subtracted from the sample data according to the buffer mass contribution. Inspection of the data shown in Fig. 1 reveals that the dynamical behavior of PS II membrane fragments hydrated at 57% r.h. is characterized by two distinct temperature regions. While there is only a slight linear increase of $\langle u^2 \rangle$ with increasing temperature below ~240 K, a strong deviation is observed above ~240 K, where $\langle u^2 \rangle$ increases linearly with a much steeper slope (see full squares in Fig. 1). This feature is the signature of the dynamical transition in proteins and membranes [53]. In contrast, the $\langle u^2 \rangle$-values of the sample equilibrated at 44% r.h. increase almost linearly with increasing temperature within the whole range from 100 K to 280 K (see open triangles in Fig. 1). Thus, it can be concluded that the dynamical transition is absent at the hydration level of 44% r.h. As also shown in Fig. 1, the increase of electron transfer efficiency from $Q_A^{-\bullet}$ to Q_B with increasing temperature (data taken from [10]) strictly correlates with the dynamical transition of PS II membrane fragments hydrated at 57% r.h. The observed phenomenon provides further evidence for our previous finding of a hydration-dependent "dynamical transition" [41] and for an onset of localized conformational motions above 44% r.h. in PS II membrane fragments at room temperature [42]. It should be mentioned, however, that the latter data were obtained at a different resolution corresponding to motions at a time scale of ~20 ps in comparison to ~100 ps in the present study. In summary, it can be concluded that dehydration of PS II membrane fragments leads to "freezing" of protein flexibility and to a concomitant inhibition of electron transfer from $Q_A^{-\bullet}$ to Q_B as similarly observed for a number of other proteins or protein–lipid systems [32,34–36].

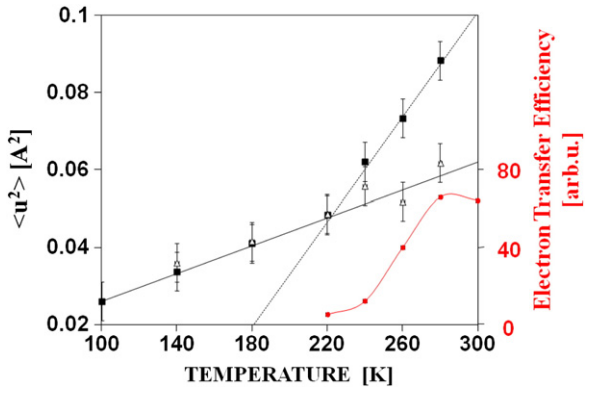

Fig. 1. Temperature dependence of the average atomic mean square displacement $\langle u^2 \rangle$ obtained for PS II membrane fragments hydrated at 57% r.h. (full squares) and 44% r.h. (open triangles). The full lines are given as a guide to the eye. The increase of electron transfer efficiency from Q_A^- to Q_B taken from Renger et al. [10] (red line) with increasing temperature strictly correlates with the dynamical transition.

Interestingly, there is evidence for a similar dynamics-function correlation in type II reaction centers of purple bacteria (PBRC) but the threshold temperature of the transition is lower [54]. The structure of the acceptor side of PBRC (for a review, see Lancaster [55]) exhibits striking similarities to that of PS II except of the coordination of the non-heme iron (NHFe) by glutamate in PBRC and (bi)carbonate in PS II (for a recent review, see [56]). In case of PBRC it appears likely that the triggering by conformational changes required for Q_B reduction by $Q_A^{-\bullet}$ comprises the rearrangement of hydrogen bonds, most prominently the reorientation of Ser223 of the L-subunit [55,57]. Based on the similarity of the acceptor side reactions in anoxygenic PBRC and in PS II it seems likely that an analogous conformational triggering of $Q_A^{-\bullet}$ reoxidation by Q_B exists in both systems (for a review see [4]) but some differences probably exist in the details of the structural rearrangements as reflected by different threshold temperatures [11]. Recently a change of the coordination mode of the NHFe by bicarbonate was reported to be involved in the triggering of PS II [58]. A corresponding change of the NHFe coordination by glutamate in PBRC has not been reported so far. In conclusion, these findings underline that protein dynamics on the picosecond timescale plays a key role for the reactions of oxidative water splitting and plastoquinol formation that are energetically driven by the radical ion pair $P680^{+\bullet}Q_A^{-\bullet}$ generated via light-induced charge separation in PS II [59].

3.2. IINS experiments

In order to gain information on vibrational protein dynamics, complementary IINS experiments were performed in the same temperature range covered by the EINS measurements discussed above. So far, the NERA spectrometer has been mainly used to determine distinct localized vibrational frequencies of comparatively small molecules like methanol [60] in the neutron energy transfer range between 5 and 200 meV. However, with an elastic energy resolution of ~0.7 meV it is also well suited to measure IINS spectra in the range of low-frequency protein vibrations, which typically exhibit Boson peaks in the neutron energy transfer range smaller than 20 meV.

IINS spectra were measured for a PS II membrane fragment sample hydrated at 57% r.h. and the corresponding buffer solution at temperatures of 20, 150, and 250 K in order to characterize the low-frequency vibrations. It is important to note that at this hydration level PS II membrane fragments are capable to undergo the dynamical transition (see above), and the inelastic features observed can be correlated with the dynamics unraveled by EINS (see above). The data obtained at 250 K are shown in Fig. 2 for both, PS II membrane fragments (upper blue line) and the D_2O-containing buffer solution (lower red line). In Fig. 2, the latter contribution was scaled by a factor of two in order to avoid overlap with other data shown in the figure. Both data sets reveal two broad features peaking at about 5.4 meV and at about 18.5 meV (see black arrows in Fig. 2). The buffer spectrum was subtracted from the sample spectrum according to its mass contribution. The difference spectrum

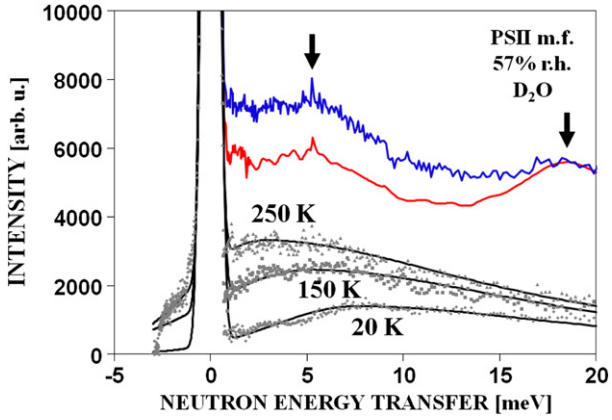

Fig. 2. IINS spectra of PS II membrane fragments hydrated at 57% r.h. (blue line) and corresponding buffer solution (red line, scaled by a factor of two for better visibility) obtained with an elastic resolution of 0.7 meV at 250 K. The difference spectra attributed to PS II membrane fragments are shown for temperature values of 20 K (gray diamonds), 150 K (gray squares), and 250 K (gray triangles). The smooth black lines are data fits calculated according to Eq. (8) (see text for details).

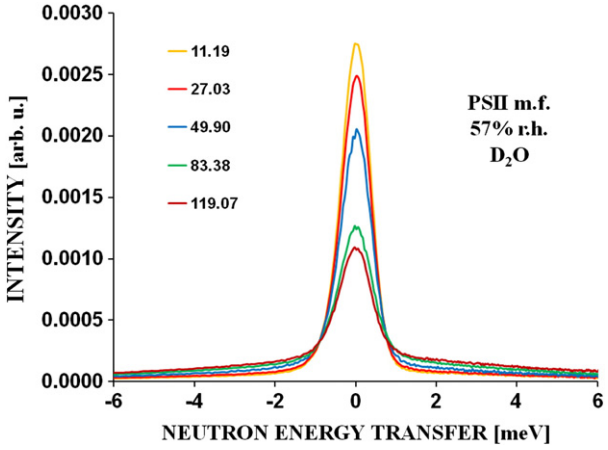

Fig. 3. IINS difference spectra of PS II membrane fragments hydrated at 57% r.h. obtained at five different scattering angles with an elastic resolution of 0.88 meV at room temperature (see inset for scattering angles). The difference between sample and buffer spectra was obtained as described in Fig. 2.

reflecting the IINS spectrum of PS II membrane fragments is displayed by gray triangles in Fig. 2. As expected, the latter spectrum exhibits typical properties of a Boson peak with a broad maximum at about 2–3 meV and a very slight tailing towards higher neutron energy transfers. On the other hand, the additional peak at ~18.5 meV vanishes, which is an indication for a proper subtraction of the buffer contribution.

The data obtained at temperatures of 20 and 150 K (not shown) were treated in the same way as described above for the 250 K data. The resulting inelastic scattering functions at 20, 150, and 250 K are displayed in Fig. 2. The shapes of the three spectra are qualitatively quite similar. Moreover, the peak position of the Boson peak at 20 K is found at ~7.5 meV, which closely resembles the values reported previously for PS II membrane fragments at low temperature [41]. However, the most remarkable finding is that the peak position shifts to lower neutron energy transfer values with increasing temperature (see below). It is important to note in this regard that the Boson peak remains distinct from the elastic peak at all temperature values under study. The latter finding proves that even at 250 K the quasielastic contribution is relatively small, so that the spectra can be fit with phenomenological scattering functions according to Eq. (8), where the one-phonon function is represented by an asymmetric profile composed of a Gaussian shape at its low-energy wing and a more slowly tailing Lorentzian shape at its high-energy side. The fit parameters are listed in detail in Table 1. According to these fits, the peak position of the Boson peak shifts from 7.5 meV at 20 K to 2.5 meV at 250 K.

For comparison further IINS experiments at room temperature were carried out at the time-of-flight spectrometer DIN-2PI using a resolution of 0.88 meV. The difference scattering functions obtained for PS II membrane fragments hydrated at 57% r.h. at selected scattering angles are shown in Fig. 3. It is apparent from this data that no distinct Boson peak can be observed at this temperature. Rather, the inelastic part of the IINS spectrum merges with the elastic and quasielastic part of the spectrum.

Table 1
Parameters of the one-phonon profiles used to fit the IINS spectra shown in Fig. 2.

		20 K	150 K	250 K
Peak phonon frequency	ω_m [meV]	7.5	5.0	2.5
FWHM of Gaussian wing	Γ_G [meV]	10	12	8
FWHM of Lorentzian wing	Γ_L [meV]	30	30	30
FWHM, one-phonon profile	Γ [meV]	20	21	19

A more detailed analysis of the QENS spectra of PS II membrane fragments is achieved by employing a phenomenological model according to Eq. (3). A magnification of the quasielastic region of the IINS spectra of Fig. 3 is shown in Fig. 4. Satisfactory fits require a model scattering function comprising a single quasielastic Lorentzian component and an elastic contribution determined in separate vanadium runs. The Lorentzian width (HWHM) of 4.06 meV was found to be independent of the momentum transfer Q. It is important to note that a Q-independent linewidth is the signature of localized conformational proton motions in the protein–lipid system under study. The width (HWHM) of 4.06 meV corresponds to a mean relaxation time ~162 fs. More generally, a broad and widely continuous distribution of relaxation times and corresponding linewidths is expected in a complex amorphous system [24,61]. Therefore, the correlation time of 162 fs has to be viewed as a mean value of the distribution of relaxation times at the given instrument resolution. The elastic intensities (EISF) approximated by the phenomenological fits described above are shown in the inset of Fig. 4 as a function of momentum transfer Q. The Q-dependence of the EISF can be well fitted with a double well jump model according to Eq. (4) (see full red line in Fig. 4). This implies that the potential

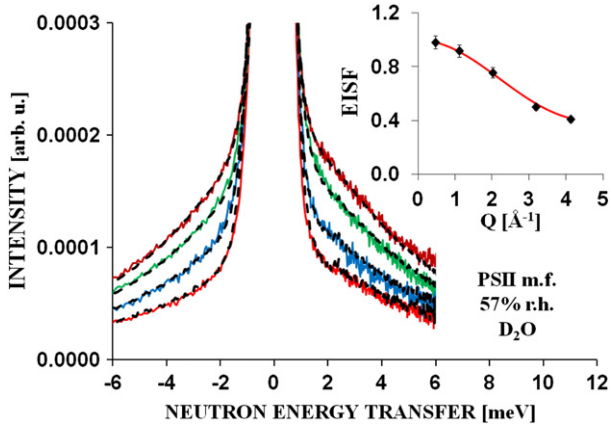

Fig. 4. Magnification of the quasielastic region of the IINS spectra shown in Fig. 3. The dashed black lines are Lorentzian fits according to Eq. (3). The inset shows the elastic incoherent structure factor obtained from the Lorentzian fits as a function of momentum transfer Q. The red line is a fit according to the double-well jump model (see Eq. (4)).

landscape of PS II membrane fragments at room temperature can be well approximated by a double well potential, where the occupation probability of the ground state potential is about 51% and the average jump distance between the two wells is 0.94 Å. The latter finding illustrates that the scattering function at room temperature is dominated by the signature of localized conformational dynamics.

The results of the present study are summarized in Fig. 5. The Boson peak energies determined above (see red points) are compared to the average atomic mean square displacements $\langle u^2 \rangle$ of PS II membrane fragments hydrated at 57% r.h. (full squares) and 44% r.h. (open triangles) obtained at a time resolution of ~100 ps in this study (taken from Fig. 1) as well as to $\langle u^2 \rangle$ of PS II membrane fragments hydrated at 90% r.h. (gray diamonds, data taken from [41]) obtained at a time resolution of ~20 ps. As discussed in our previous study (see [41] and references therein), the $\langle u^2 \rangle$-values reveal three temperature regions (see Fig. 5): region A with T<120 K is characterized by purely harmonic vibrational motions, region B with 120 K<T<230 K exhibits a slight deviation from the harmonic vibrational behavior due to the onset of methyl group rotations and finally, region C with T>230 K shows a strong increase of $\langle u^2 \rangle$ due to the presence of hydration-induced localized diffusive motions. IINS spectra of PS II membrane fragments hydrated in D_2O at 57% r.h. were measured at one temperature value in each of the three temperature regions. The IINS experiments revealed a distinct Boson peak at ~7.5 meV at 20 K, which subsequently shifts towards lower energy transfers to 2.5 meV at 250 K upon temperature increase.

This effect differs from that observed for the antenna complex LHC II, where the density of vibrational states remained virtually identical below ~120 K [17]. This is also widely assumed in the interpretation of temperature-dependent HB experiments, which are restricted to temperatures below 40 K [7]. In contrast, the deviation from this behavior observed in the case of PS II membrane fragments in temperature region B indicates a softening of the protein matrix along with the onset of conformational dynamics that leads to a shift of the mean phonon frequency. If the protein matrix is viewed as a harmonic oscillator, this effect could be rationalized as a weakening of the force constant. This finding may further imply that the density of vibrational states is affected by the transition from the crystalline-like to the amorphous state of the protein matrix observed at ~120 K and the dynamical transition at ~230 K. In consequence, this means that simulations of EET kinetics at physiological temperatures should account not only for thermal population of vibrational states, but also for a temperature-dependent density of vibrational states.

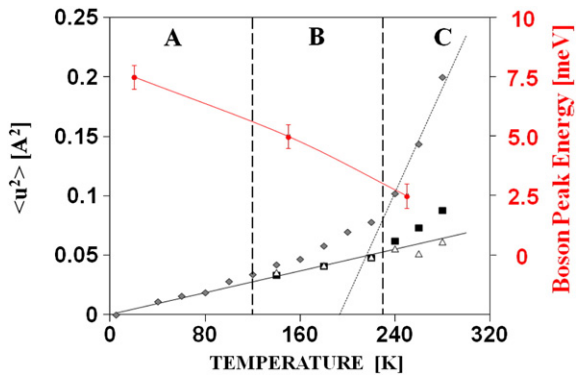

Fig. 5. Comparison of Boson peak energy (red points, taken from Fig. 2) and average atomic mean square displacements $\langle u^2 \rangle$ of PS II membrane fragments obtained at different hydration levels and time resolutions. The average atomic mean square displacements $\langle u^2 \rangle$ were acquired for PS II membrane fragments hydrated at 57% r.h. (full squares) and 44% r.h. (open triangles) at a time resolution of ~100 ps in this study (see Fig. 1) as well as for PS II membrane fragments hydrated at 90% r.h. (gray diamonds, data taken from Pieper et al. [41]) at a time resolution of ~20 ps. The straight lines are given as a guide to the eye.

It has to be kept in mind, however, that the data presented here were obtained for membrane fragments. Therefore, further experiments on isolated antenna complexes like LHC II are necessary to verify the significance of the observed effect in specialized light-harvesting complexes. Nevertheless, the data presented here from NERA and DIN-2PI measurements nicely demonstrate that IINS is capable of providing valuable quantitative information on the vibrational dynamics of pigment–protein complexes not only at low, but also at physiological temperatures.

Acknowledgement

J. Pieper gratefully acknowledges support by the European Social Fund's Internationalisation Programme DoRa. Financial support by Estonian Science Foundation (grant no 9453), Deutsche Forschungsgemeinschaft (SFB 429, TP A1), ILL Grenoble, and from JINR Dubna is gratefully acknowledged. M. Trapp was supported by a PhD scholarship from the French Ministry for Research and Technology. We are also grateful to S. Kussin and M. Weß (TU Berlin) for their help in sample preparation, to Dr. A.V. Puchkov for his support as well as to D. Nowak and V.M. Morozov for their assistance during the neutron scattering experiments.

References

[1] B. Green, W.W. Parson (Eds.), Light Harvesting Antennas, Advances in Photosynthesis and Respiration, vol. 13, Springer, Dordrecht, 2003.
[2] G. Renger (Ed.), Primary Processes of Photosynthesis: Principles and Apparatus, Part I Photophysical Principles, Pigments and Light Harvesting/Adaptation/Stress, Royal Society Chemistry, Cambridge, 2008.
[3] R. Jankowiak, M. Reppert, V. Zazubovich, J. Pieper, T. Reinot, Site selective and single complex laser-based spectroscopies: a window on excited state electronic structure, excitation energy transfer, and electron–phonon coupling of selected photosynthetic complexes, Chem. Rev. 111 (2011) 4546–4598.
[4] G. Renger, Photosynthetic water splitting: apparatus and mechanism, in: J. Eaton-Rye, Tripathy, T.D. Sharkey (Eds.), Photosynthesis: Plastid Biology, Energy Conversion and Carbon Assimilation, Springer, Dordrecht, The Netherlands, 2011, pp. 359–414.
[5] T. Renger, A.R. Holzwarth, Theory of excitation energy transfer and optical spectra of photosynthetic systems, Advances in Photosynthesis and Respiration 26 (5) (2008) 421–443.
[6] R. Purchase, S. Völker, Spectral hole burning: examples from photosynthesis, Photosynth. Res. 101 (2009) 245–266.
[7] J.M. Hayes, P.A. Lyle, G.J. Small, A theory for the temperature dependence of hole-burned spectra, J. Phys. Chem. 98 (1994) 7337–7341.
[8] J.L. Hughes, P. Smith, R. Pace, E. Krausz, Charge separation in photosystem II core complexes induced by 690–730 nm excitation at 1.7 K, Biochim. Biophys. Acta 1757 (2006) 841–851.
[9] P. Joliot, A. Joliot, Different types of quenching involved in photosystem II centers, Biochim. Biophys. Acta 305 (1973) 302–316.
[10] G. Renger, H.M. Gleiter, E. Haag, F. Reifarth, Photosystem II: thermodynamics and kinetics of electron transport and deleterious effects of copper (II), Z. Naturforsch. 48c (1993) 234–240.
[11] A. Garbers, J. Kurreck, F. Reifarth, G. Renger, F. Parak, Correlation between protein flexibility and electron transfer from Q_A^- to Q_B in PS II membrane fragments from spinach, Biochemistry 37 (1998) 11399–11404.
[12] G. Renger, Coupling of electron and proton transfer in oxidative water cleavage in photosynthesis, Biochim. Biophys. Acta 1655 (2004) 195–204.
[13] O. Kaminskaya, G. Renger, V.A. Shuvalow, Effect of dehydration on light induced reactions in photosystem II: photoreactions of cytochrome b559, Biochemistry 42 (2003) 8119–8132.
[14] T. Noguchi, M. Sugiura, Flash-induced FTIR difference spectra of the water oxidizing complex in moderately hydrated photosystem II core films: effect of hydration extent on S-state transitions, Biochemistry 41 (2002) 2322–2330.
[15] J.C. Smith, Protein dynamics: comparison of simulations with inelastic neutron scattering experiments, Q. Rev. Biophys. 24 (1991) 1–65.
[16] A. Orecchini, A. Paciaroni, A.R. Bizzarri, S. Cannistraro, Low-frequency vibrational anomalies in ß-lactoglobulin: contribution of different hydrogen classes revealed by inelastic neutron scattering, J. Phys. Chem. B 105 (2001) 12150–12156.
[17] J. Pieper, K.-D. Irrgang, G. Renger, R.E. Lechner, Density of vibrational states of the light-harvesting complex II of green plants studied by inelastic neutron scattering, J. Phys. Chem. B 108 (2004) 10556–10565.
[18] A. Paciaroni, S. Cinelli, G. Onori, Effect of the environment on the protein dynamical transition: a neutron scattering study, Biophys. J. 83 (2002) 1157–1164.
[19] J. Pieper, M. Rätsep, R. Jankowiak, K.-D. Irrgang, J. Voigt, G. Renger, G.J. Small, Qy-level structure and dynamics of solubilized light-harvesting complex II of green plants: pressure and hole burning studies, J. Phys. Chem. A 103 (1999) 2412–2421.

[20] J. Pieper, R. Schödel, M. Rätsep, R. Jankowiak, K.-D. Irrgang, J. Voigt, G. Renger, Electron–phonon coupling in solubilized LHC II complexes of green plants investigated by line-narrowing and temperature-dependent fluorescence spectroscopy, J. Phys. Chem. B 105 (2001) 7115–7124.
[21] H. Frauenfelder, G. Chen, J. Berendzen, P.W. Fenimore, H. Jansson, B.H. McMahon, I.R. Stroe, J. Swenson, R.D. Young, A unified model of protein dynamics, Proc. Natl. Acad. Sci. U. S. A. 106 (2009) 5129–5134.
[22] J. Fitter, R.E. Lechner, N.A. Dencher, Interactions of hydration water and biological membranes studied by neutron scattering, J. Phys. Chem. B 103 (1999) 8036–8050.
[23] F. Gabel, D. Bicout, U. Lehnert, M. Tehei, M. Weik, G. Zaccai, Protein dynamics studied by neutron scattering, Q. Rev. Biophys. 35 (2002) 327–367.
[24] G. Kneller, Quasielastic neutron scattering and relaxation processes in proteins: analytical and simulation-based models, Phys. Chem. Chem. Phys. 7 (2005) 2641–2655.
[25] W. Doster, S. Cusack, W. Petry, Dynamical transition of myoglobin revealed by inelastic neutron scattering, Nature 337 (1989) 754–756.
[26] J. Zaccai, How soft is a protein? A protein force constant measured by neutron scattering, Science 288 (2000) 1604–1607.
[27] M. Tarek, T. Tobias, The role of protein–water hydrogen bonds in the dynamical transition of proteins, Phys. Rev. Lett. 88 (2002) 381011–381013.
[28] S.-H. Chen, L. Liu, E. Fratini, P. Baglioni, A. Faraone, E. Mamontov, Observation of fragile-to-strong dynamic crossover in protein hydration water, Proc. Natl. Acad. Sci. U. S. A. 103 (2006) 9012.
[29] S. Khodadadi, S. Pawlus, J.H. Roh, V. Garcia Sakai, E. Mamontov, A.P. Sokolov, The origin of the dynamic transition in proteins, J. Chem. Phys. 128 (2008) 195106.
[30] S. Magazu, F. Migliardo, A. Benedetto, Puzzle of protein dynamical transition, J. Phys. Chem. B 115 (2011) 7736–7743.
[31] W. Doster, S. Busch, A.M. Gaspar, M.-S. Appavou, J. Wuttke, H. Scheer, Dynamical transition of protein–hydration water, Phys. Rev. Lett. 104 (2010) 098101.
[32] M. Ferrand, A.J. Dianoux, W. Petry, G. Zaccai, Thermal motions and function of bacteriorhodopsin in purple membranes: effects of temperature and hydration studied by neutron scattering, Proc. Natl. Acad. Sci. U. S. A. 90 (1993) 9668–9672.
[33] F. Natali, A. Relini, A. Gliozzi, R. Rolandi, P. Cavatorta, A. Deriu, A. Fasano, P. Riccio, The influence of the lipid–protein interaction on the membrane dynamics, Physica B 350 (2004) 623–626.
[34] U. Lehnert, V. Réat, M. Weik, G. Zaccai, C. Pfister, Thermal motions in bacteriorhodopsin at different hydration levels studied by neutron scattering, Biophys. J. 75 (1998) 1945–1952.
[35] J. Fitter, The temperature dependence of internal molecular motions in hydrated and dry alpha-amylase: the role of hydration water in the dynamical transition of proteins, Biophys. J. 76 (1999) 1034–1042.
[36] M. Trapp, T. Gutberlet, F. Juranyi, T. Unruh, B. Demé, M. Tehei, J. Peters, Hydration dependent studies of highly aligned multilayer lipid membranes by neutron scattering, J. Chem. Phys. 133 (2010) 164505.
[37] J. Fitter, S.A.W. Verclas, R.E. Lechner, H. Seelert, N.A. Dencher, Function and picosecond dynamics of bacteriorhodopsin in purple membrane at different lipidation and hydration, FEBS Lett. 433 (1998) 321–325.
[38] L. Cordone, M. Ferrand, E. Vitrano, G. Zaccai, Harmonic behavior of trehalose-coated carbon-monoxy-myoglobin at high temperature, Biophys. J. 76 (1999) 1043–1047.
[39] A. Paciaroni, A. Orecchini, S. Cinelli, G. Onori, R.E. Lechner, J. Pieper, Protein dynamics on the picosecond timescale as affected by the environment: a quasielastic neutron scattering study, Chem. Phys. 292 (2003) 397–404.
[40] M. Marconi, A. de Francesco, E. Cornicchi, G. Onori, A. Paciaroni, Hydration and temperature dependent dynamics of lysozyme in glucose–water matrices. A neutron scattering study, Chem. Phys. 317 (2005) 274–281.
[41] J. Pieper, T. Hauß, A. Buchsteiner, K. Baczynski, K. Adamiak, R.E. Lechner, G. Renger, Temperature- and hydration-dependent protein dynamics in photosystem II of green plants studied by quasielastic neutron scattering, Biochemistry 46 (2007) 11398–11409.
[42] J. Pieper, T. Hauß, A. Buchsteiner, G. Renger, The effect of hydration on protein flexibility in photosystem II of green plants studied by quasielastic neutron scattering, Eur. Biophys. J. 37 (2008) 657–663.
[43] J. Pieper, G. Renger, Protein dynamics investigated by neutron scattering, Photosynth. Res. 102 (2009) 281–293.
[44] G. Nagy, J. Pieper, S. Krumova, L. Kovács, M. Trapp, G. Garab, J. Peters, Dynamic properties of photosystem II membranes at physiological temperatures characterized by elastic incoherent neutron scattering. Increased flexibility associated with the inactivation of the oxygen evolving complex, Photosynth. Res. 111 (2012) 113–124.
[45] D.A. Berthold, G.T. Babcock, C.F. Yocum, A highly resolved, oxygen-evolving photosystem II preparation from spinach thylakoid membranes: EPR and electron-transport properties, FEBS Lett. 134 (1981) 231–234.
[46] M. Völker, T. Ono, Y. Inoue, G. Renger, Effect of trypsin on PS II particles. Correlation between Hill-activity, Mn-abundance and peptide pattern, Biochim. Biophys. Acta 767 (1985) 548–556.
[47] F. Natali, J. Peters, D. Russo, S. Barbieri, C. Chiapponi, A. Cupane, A. Deriu, M.T. Di Bar, E. Fahi, Y. Gerelli, P. Mariani, A. Paciarioni, C. Rivasseau, G. Schiro, F. Sonvico, IN13 backscattering spectrometer at ILL: looking for motions in biological macromolecules and organisms, Neutron News 19 (2008) 14–18.
[48] D. Richard, M. Ferrand, G.J. Kearley, Analysis and visualisation of neutron-scattering data, J. Neutron Res. 4 (1996) 33–39.
[49] I. Natkaniec, S.I. Bragin, J. Brankowski, J. Mayer, in: U. Steigenberger, T. Broome, G. Ress, A. Soper (Eds.), Proceedings of the XIIth Meeting on International Collaboration on Advanced Neutron Sources, Rutherford Appleton Laboratory Report 94–025, vol. 1, 1994, p. 89.
[50] M. Bée, Quasielastic Neutron Scattering: Principles and Applications in Solid State Chemistry, Biology Materials Science, Adam & Hilger, Philadelphia, 1988.
[51] A. Stoeckli, A. Furrer, C. Schoenenberger, B.H. Meier, R.R. Ernst, I. Anderson, Dynamics of hydrogen bonds in carboxylic acids, Physica B 136 (1986) 161–164.
[52] R.E. Lechner, C. Riekel, Neutron Scattering and Muon Spin Rotation, Springer Verlag, Berlin, Heidelberg, New York, Tokyo, 1983.
[53] W. Doster, The dynamical transition of proteins, concepts and misconceptions, Eur. Biophys. J. 37 (2008) 591–602.
[54] F. Parak, E.N. Frolov, A.A. Kononenko, R. Mössbauer, V.I. Goldansky, A.B. Rubin, Evidence for a correlation between the photoinduced electron transfer and dynamic properties of the chromatophore membranes from *Rhodospirillum rubrum*, FEBS Lett. 17 (1980) 368–372.
[55] C.R.D. Lancaster, Structures of reaction centers in anoxygenic bacteria, in: G. Renger (Ed.), Primary Processes of Photosynthesis: Basic Principles and Apparatus, Vol. II Reaction Centers/Photosystems, Electron Transport Chains, Photophosphorylation and Evolution, Royal Society Chemistry, Cambridge, 2007, pp. 5–56.
[56] F. Müh, C. Glöckner, J. Hellmich, A. Zouni, Light-induced quinone reduction in photosystem II, Biochim. Biophys. Acta 1817 (2012) 44–65.
[57] A.Y. Mulkidjanian, M.A. Kozlova, D.A. Cherepanov, Ubiquinone reduction in the photosynthetic reaction centre of *Rhodobacter sphaeroides*: interplay between electron transfer, proton binding and flips of the quinone ring, Biochem. Soc. Trans. 33 (2005) 845–850.
[58] P. Chernev, I. Zaharieva, H. Dau, M. Haumann, Carboxylate shifts steer interquinone electron transfer in photosynthesis, J. Biol. Chem. 286 (2011) 5368–5374.
[59] G. Renger, A.R. Holzwarth, Primary electron transfer, in: T. Wydrzynski, K. Satoh (Eds.), Photosystem II: the Water/Plastoquinone Oxido-reductase in Photosynthesis, Kluwer Academic Publishers, Dordrecht, The Netherlands, 2005, pp. 139–175.
[60] I. Natkaniec, K. Holderna-Natkaniec, I. Majerz, K. Parlinski, Neutron spectroscopy of deuterated substitutes and DFT modeling vibrational spectra of methanol clusters, Chem. Phys. 317 (2005) 171–177.
[61] W. Doster, M. Settles, Protein–water displacement distributions, Biochim. Biophys. Acta 1749 (2005) 173–186.